

## Electronic Supplementary Information

### Hybrid Plasmonic Metasurface as Enhanced Raman Hot-Spots for Pesticide Detection at Ultralow Concentrations

Yazan Bdour,<sup>a</sup> Graham Beaton,<sup>b</sup> Juan Gomez-Cruz,<sup>a</sup> Oscar Cabezuelo,<sup>b</sup> Kevin Stamplecoskie<sup>b</sup> and Carlos Escobedo<sup>\*a,b</sup>

#### Materials and Methods

##### Nanohole Arrays

The metallic nanohole arrays (NHAs) were fabricated from PELCO holey 100-nm-thick silicon nitride membranes containing holes of 200 nm in diameter and 200 nm periodicity, spanning  $500 \times 500 \mu\text{m}^2$  (Ted Pella, Redding, CA, USA). The membranes were coated with a thermally evaporated **5 nm** layer of Cr, followed by 100 nm thick layer of Au using a 3 kW Linear e-gun physical vapour deposition evaporator (Thermionics, Hayward, CA) at Nanofabrication Kingston. The NHAs were optically inspected using an FEI-MLA Qunata 650 FEG-ESEM available at Queen's Facility for Isotope Research (Queen's University, Kingston, ON).

##### Experimental Setup

The chip assembly consists of two merged microfluidics chips that were designed using computer aided design software (SolidWorks, Dassault Systems) and 3D-printed using ANYCUBIC PHOTON S (Shenzhen, Guangdong, China). Sylgard 184 polydimethyl-siloxane (PDMS) (Dow Corning) mixed at 10:1 ratio, and baked at **70 °C** on a hot plate for 3 hrs was used to create the microchannels. The top layer was punched with a **1 mm** biopsy tool to provide access to the Pt wire electrode. The bottom layer was punched with a **3 mm** biopsy tool to securely host the NHAs. Rhodamine 6G (R6G) was purchased from Millipore Sigma (Oakville, ON, Canada). A 10<sup>-3</sup> M R6G solution was pumped through the channels into the assembly using a **10 μL** pipette.

##### Raman spectroscopy

All spectra were recorded using an Ocean Optics micro-ID Raman (785 nm, 10.5 mW) system equipped with a 40× objective. Spectra acquisition was conducted at 6 different locations over the NHAs, with an integration time of **5 s**. The spectra are averaged, and then normalized to the highest obtained peak.

## R6G Raman Signal on Thin Au Film

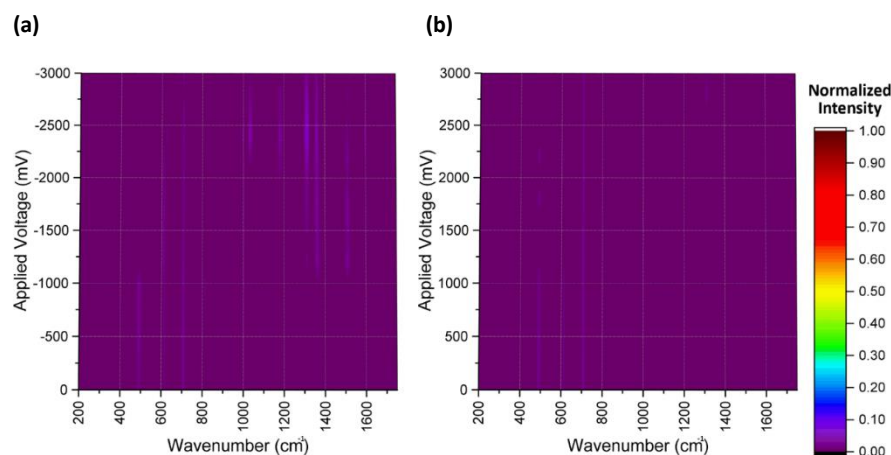


Figure SI 1. Normalized contour map of the Raman signal intensities of R6G on a thin Au film (a) under negative applied potential, (b) under positive applied potential.

## Average Enhancement Factor

The enhancement factor requires an estimated value of the Raman laser penetration depth, which can be proportional to the laser spatial resolution,  $\lambda/(NA)^2$ .  $\lambda$ , is the wavelength of the illuminating light and  $NA$  is the numerical aperture. Typically for a Raman microscope, at 785 nm of laser light will penetrate 12  $\mu\text{m}$  on a silicon wafer at ideal conditions.<sup>1</sup> However, due to the experimental setup, causing light scattering and focal length variance, leading to deformation within laser profile; thus reducing its penetration depth. A conservative estimate of the penetration factor is used of 11  $\mu\text{m}$  rather than 12  $\mu\text{m}$ , yielding a conservative enhancement factor of 20.45 rather than 22.31.

The enhancement factor is calculated at  $623\text{ cm}^{-1}$ ,  $839\text{ cm}^{-1}$ ,  $925\text{ cm}^{-1}$ ,  $999\text{ cm}^{-1}$ ,  $1031\text{ cm}^{-1}$ ,  $1180\text{ cm}^{-1}$ ,  $1278\text{ cm}^{-1}$ ,  $1307\text{ cm}^{-1}$ ,  $1358\text{ cm}^{-1}$ , and  $1596\text{ cm}^{-1}$  wavenumbers. The maximum enhancement factor is found at  $1031\text{ cm}^{-1}$ . The average enhancement factor is calculated by firstly averaging the enhancement factor of each wavenumber across all applied potentials, then averaging once again across all wavenumbers. Table SI 1 summarizes all average enhancement factors.

Wavenumber ( $\text{cm}^{-1}$ )	Average Enhancement Factor				
	NHA	NP1-Au Film	NP2- Au Film	NP1-NHA	NP2-NHA
623	1.24E+06	7.77E+05	4.14E+06	1.05E+08	9.15E+07
839	1.12E+06	5.05E+05	1.05E+06	7.54E+07	6.72E+07
925	1.34E+06	4.69E+05	9.15E+05	1.49E+08	1.00E+08
999	1.38E+06	1.55E+06	2.94E+06	4.81E+07	5.60E+07
1031	2.21E+06	2.65E+06	1.15E+07	3.26E+08	2.57E+08
1180	1.92E+06	3.58E+05	1.01E+06	2.72E+07	2.83E+07
1278	1.77E+06	1.00E+06	3.25E+06	1.09E+08	3.28E+07
1307	1.81E+06	5.38E+05	1.53E+06	3.64E+07	2.97E+07
1358	2.30E+06	2.34E+05	5.65E+05	8.59E+06	5.42E+06
1596	3.86E+06	5.45E+05	1.64E+06	6.67E+07	4.86E+07
<b>Average</b>	1.90E+06	8.63E+05	2.86E+06	9.51E+07	7.16E+07

Table SI 1. Average EF of R6G obtained across different substrates.

## NP deposition on NHA

Observed particle deposition, acquired using the Raman microscope, during experiments. The images indicate particle deposition in the vicinity of the NHAs upon the application of the electric potential, during data acquisition. At relatively high potentials ( $> \pm 2.80 V$ ), the particles were observed to aggregate at the surface of the Au thin film, as well as the NHAs.

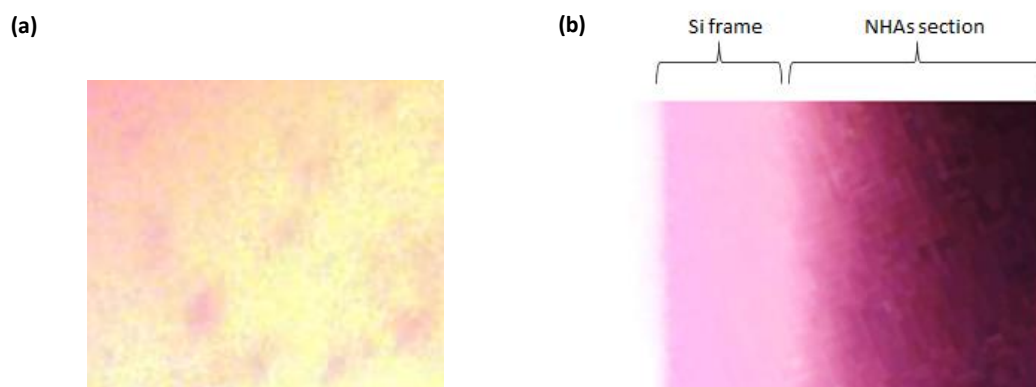


Figure SI 2. Microscope images obtained through the Raman lens of NP2 aggregation at 3.00 V applied potential on (a) Au thin film and (b) NHAs.

## Nanoparticles

For the synthesis of spherical silver nanoparticle seeds, solutions of 0.2 mM AgNO<sub>3</sub>, 1 mM trisodium citrate and 0.2 mM Omnirad-2959 (photoinitiator) were prepared. Upon excitation with UVA light, the photoinitiator can undergo a Norrish II cleavage to produce ketyl radicals capable of reducing Ag<sup>+</sup> to Ag<sup>0</sup>. The solutions were combined and purged under N<sub>2</sub> flow for ~30 minutes to remove oxygen quenching. The solution was irradiated under UVA light for ~10 minutes, until yellow in color, indicating the formation of spherical silver nanoparticles.

These spherical seeds were then taken forward for photochemical shape control to generate the larger structures used for the SERS studies. 15 mL solutions containing 4.0 mM trisodium citrate and nanoparticle seeds were irradiated for 14 hours, open to atmosphere, with a Luzchem LED illuminator with varied excitation wavelengths. 625 nm and 825 nm light were used to generate the smaller and larger nanoparticle plates, respectively.

The nanoparticle size distribution measurements were carried out on Transmission electron microscopy (TEM) image analysis. The particles were imaged using a TALOS F200i transmission electron microscope operated at an acceleration voltage of 200 kV. The samples were prepared as an aqueous dispersion on a copper grid.

The TEM image study was done with ImageJ pixel measurements, where the distributions show a high size disparity for both nanoparticle dispersions. NP1 are composed of triangular and hexagonal plates, presented in Figure SI 3 (a). While NP2 share some of the shapes of NP1, but also include cylindrical ones, shown in Figure SI 3 (b). The TEM size distribution measurements determine a size of  $35.77 \pm 1.21 \text{ nm}$  for NP1, and  $37.38 \pm 3.07 \text{ nm}$  for NP2.

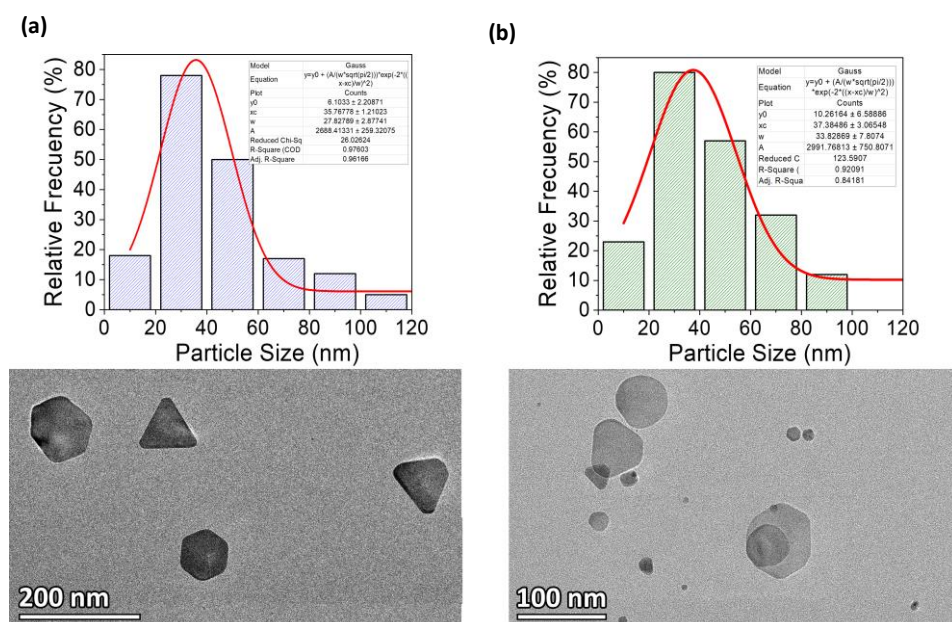


Figure SI 3. A bar graph presenting the size distribution and a TEM image of (a) NP1 (b) NP2.

## SEM and TEM Imaging

The hybrid metastructures were observed under using scanning electron microscopy (SEM) and scanning transmission electron microscopy (S-TEM). The SEM images were obtained using a Quanta 250 scanning electron microscope operated at 20.0 kV, and the S-TEM images were acquired using the TALOS F200i transmission electron microscope operated at an acceleration voltage of 200 kV. Two separate samples were prepared as described in the experimental setup at 2.5 V applied potential using NP1 and NP2, respectively. Images from multiple devices used under different conditions were acquired. Representative images of the different devices and conditions are shown in the images below. A reference NHA platform unutilized in any experimental setup, or NP dispersions imaged using an SEM and S-TEM, is presented in Figure SI 4 (a) and SI 4 (b), respectively. Figure SI 5 shows a S-TEM image of a metasurface fabricated with NHA and NP1. In this image, the nanoparticles can be observed adjacent to the edge of the NHs, with their edges aligned to the rims. Similarly, a S-TEM image of a hybrid metasurface using NHA and NP2 is shown in Figure SI 6.

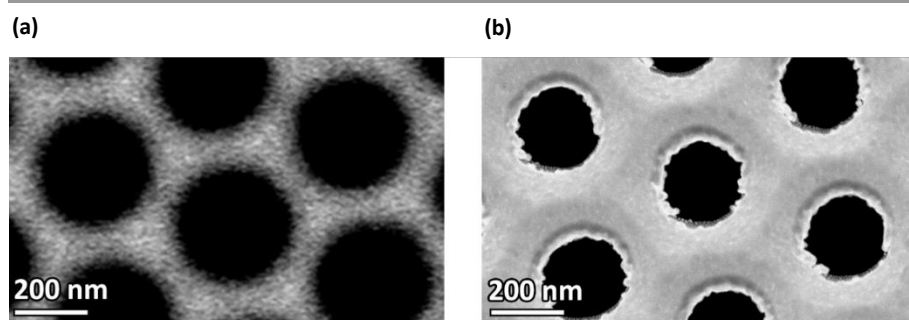


Figure SI 4. An unutilized NHA platform imaged under (a) SEM, and (b) S-TEM.

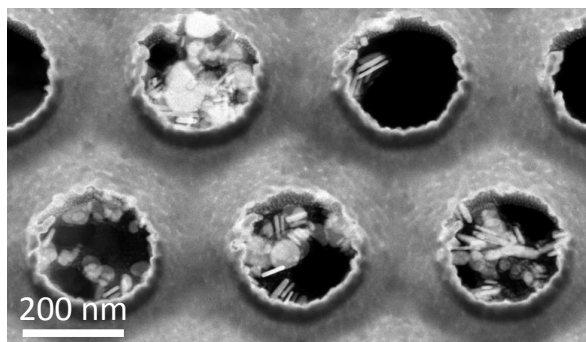


Figure SI 5. S-TEM image of nanoholes with assembled NP1 at an applied electric potential of 2.5 V.

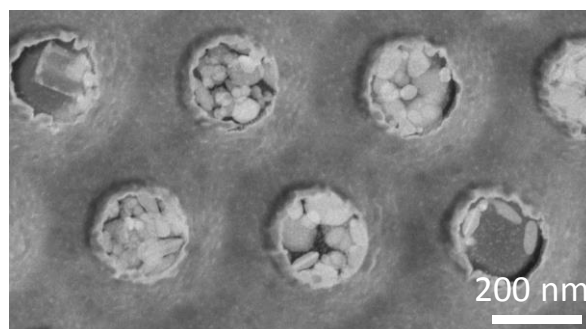


Figure SI 6. Three close-up S-TEM images of separate nanoholes decorated with NP2 at 2.5 V applied electric potential.

### Repeatability and Reproducibility

Two new experiments were carried out to show the repeatability of the reproducibility of R6G peak enhancements on separate new devices. The measurements were carried out on 6 mapped locations on the NHAs as indicated in Figure SI 7. The R6G Raman spectra for new, independent devices is presented in Figure SI 8. The intensity of the Raman spectra is normalized to the peak intensities presented in the main manuscript.

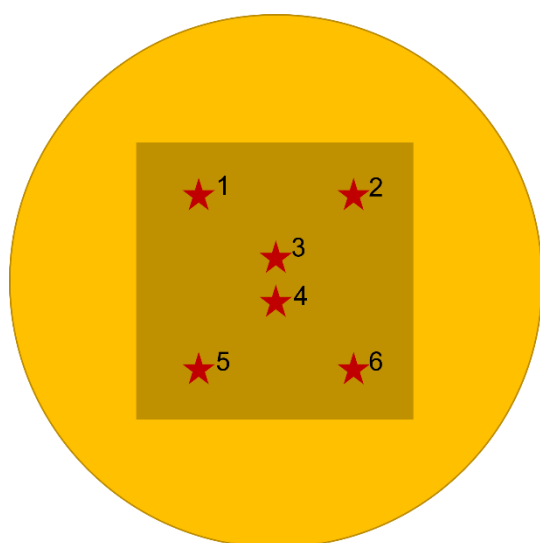


Figure SI 7. An illustration of an NHA-NP device indicating an approximate location of each spot the Raman spectra is acquired and mapped at various applied potentials.

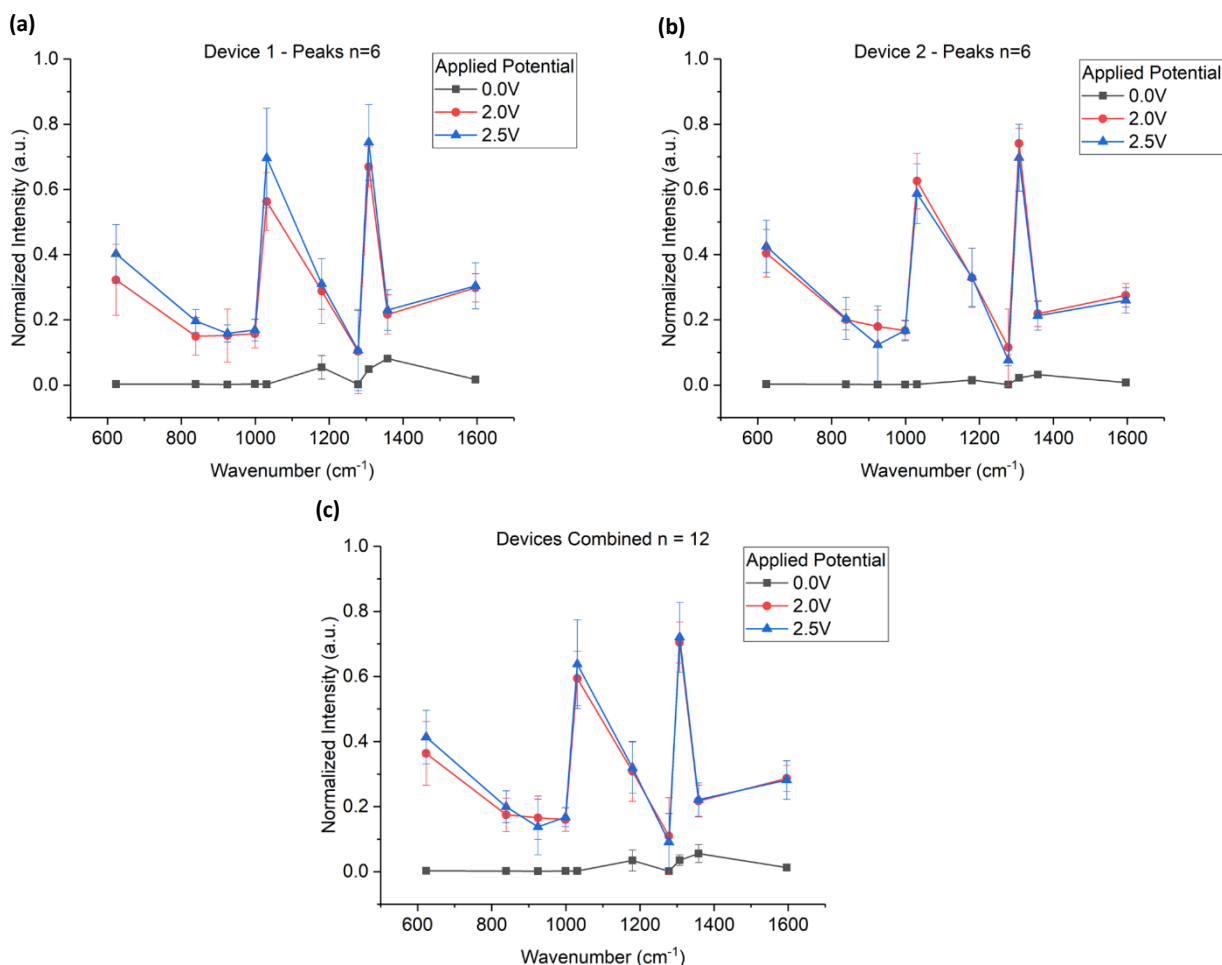
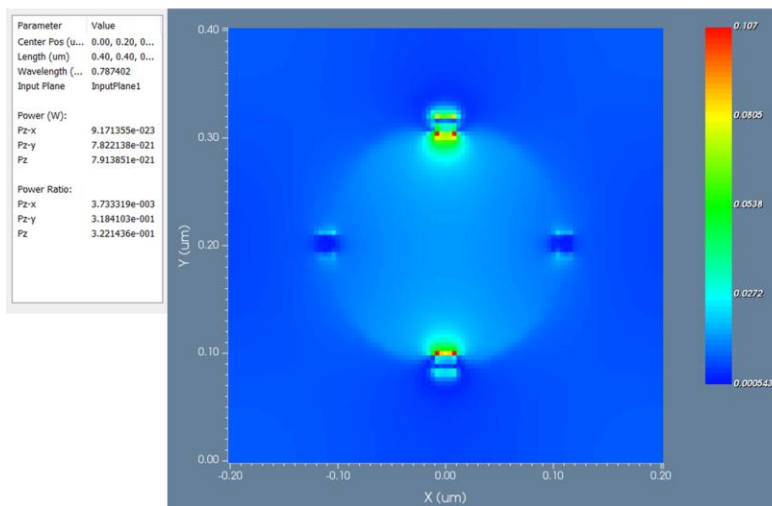


Figure SI 8. R6G normalized peaks intensity variability obtained from (a) Device 1, (b) Device 2 averaged out from 6 mapped out locations across the NHAs, highlighting the reproducibility and the repeatability of the enhancement. The variability from the devices in (c) are further compared when averaged out across the 12 spots from the combined devices.

## Simulations

FDTD simulations were carried out on the structures to highlight the plasmonic response from each device. Nanohole array structures with dimensions of 200 nm diameter, 400 nm periodicity on 500 nm SiN<sub>2</sub> and 50 nm Au, were simulated using an active region with a 4 nm mesh grid spacing. Prism shape nanoparticles with dimensions of 15 nm x 15 nm x 8 nm. Periodic boundary conditions (PBC) are used for the x and y axes boundaries to model the periodic nature of the NHAs, while perfect match layer (PML) boundary conditions are used in the z-direction to avoid light reflection from the propagation direction. The electromagnetic field was acquired through an observation area. The light source uses an input plane field with a y-axis polarized plane wave centered at 785 nm wavelength. The top view and 3D contour plots of the results are displayed in Figure SI 9 (a) and (b), respectively.

(a)



(b)

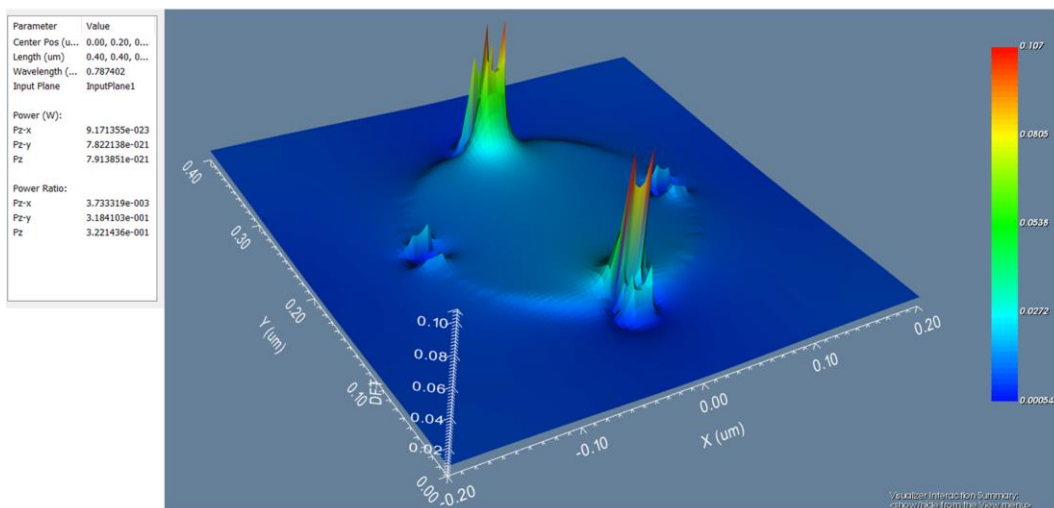


Figure SI 9. FDTD simulations showing (a) 2D top-view, (b) 3D contour plots of the plasmonic response of NPs on the rim of NH.

## Malachite Green Raman Detection

Malachite Green oxalate salt (MG) was purchased from Millipore Sigma (Oakville, ON, Canada) and diluted to **10  $\mu\text{M}$** , **100  $\text{nM}$** , and **1  $\text{nM}$**  concentrations. The spectra, presented in Figure SI 10, were recorded using an Ocean Optics micro-ID Raman (633 nm, 10.5 mW) system equipped with 40 $\times$  objective. Each concentration was recorded on separate devices, where the average spectrum was obtained at 6 different locations across the NHAs across three different applied potentials, using **10 s** integration time. The spectra are averaged and normalized to the highest obtained peak.

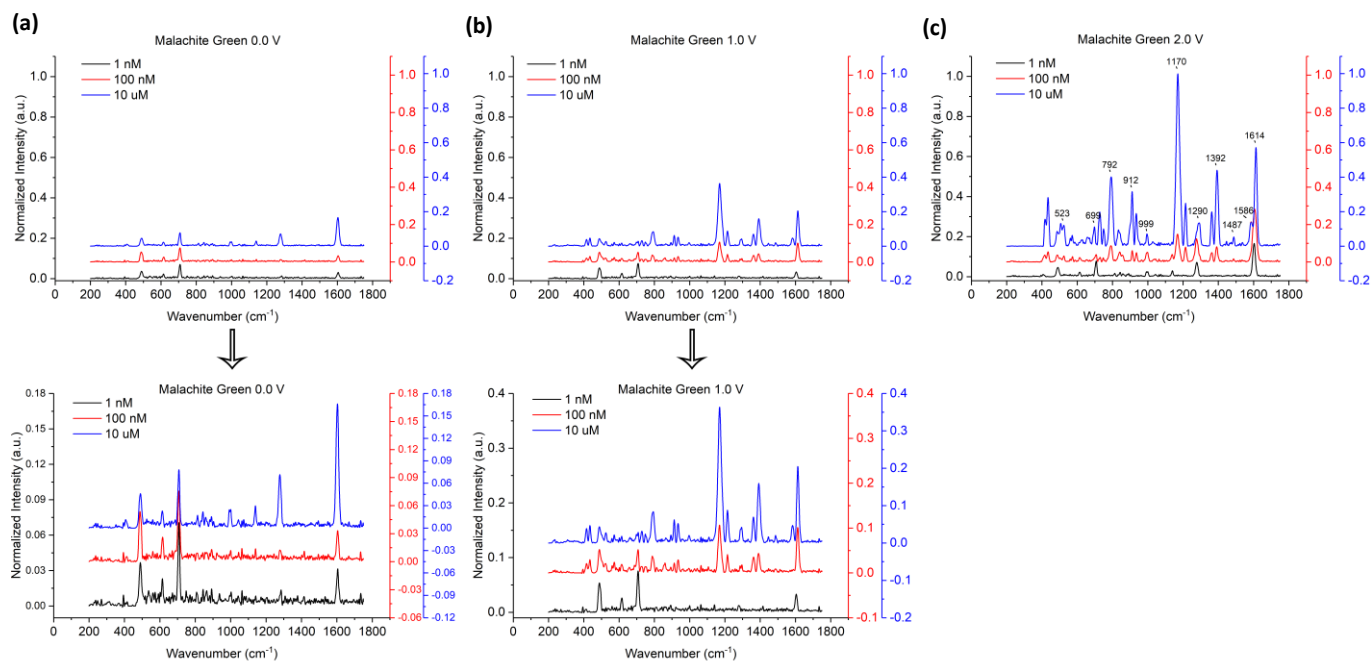


Figure SI 10. The normalized Raman spectra of MG observed at  $10\ \mu\text{M}$ ,  $100\ \text{nM}$ , and  $1\ \text{nM}$  concentrations under a)  $0.0\ \text{V}$  applied potential, b)  $1.0\ \text{V}$  applied potential, and c)  $2.0\ \text{V}$  applied potential.

## Variable Instrument Conditions

The laser power of  $10.5\ \text{mW}$  and integration time of  $5\ \text{s}$  were chosen, as it was the best conditions to obtain the R6G Raman spectra without oversaturating the instrument. To highlight the oversaturation issues, Figure SI 11 presents R6G Raman spectra at the NHAs site under  $2.0\ \text{V}$  applied potential with different laser powers, and integration times.

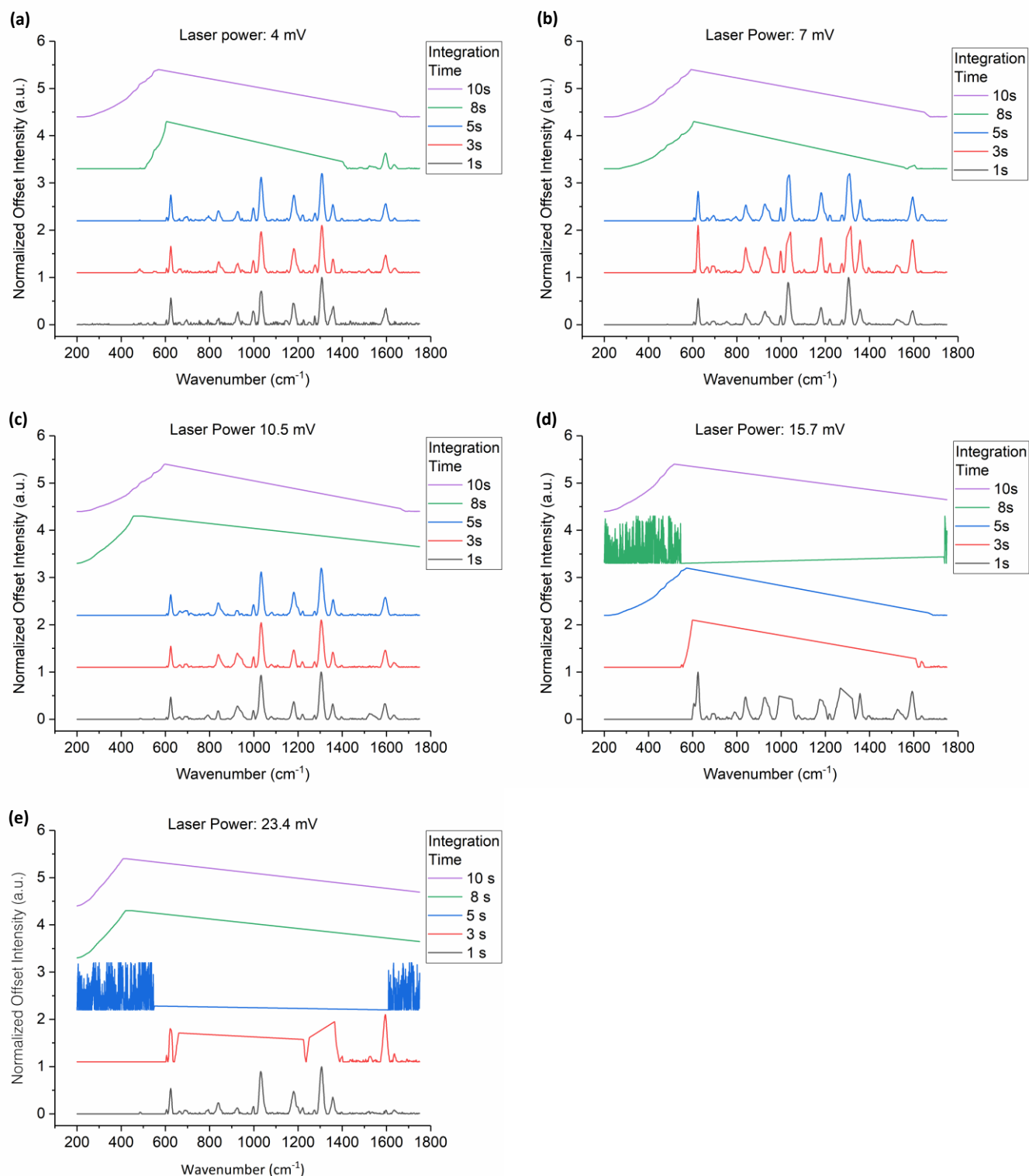


Figure SI 11. R6G Raman spectra obtained at the NHAs, while under 2.0 applied potentials with various instrumental settings, where the laser power used is, (a) 4 mV, (b) 7 mV, (c) 10.5 mV, (d) 15.7 mV, and (e) 23.4 mV, exposed for 1 s, 3 s, 5 s, 8 s, 10 s of integration time.

## Reference

1. F. Adar, *Spectroscopy*, 2010, **25**, 23.